Dynamic Analysis of Planar Solid Oxide Fuel Cell Models With Different Assumptions of Temperature Layers

Handa Xi

Jing Sun[1]

Department of Naval Architecture and Marine Engineering,
University of Michigan,
Ann Arbor, MI 48109

As solid oxide fuel cell (SOFC) technology is rapidly evolving, high-fidelity mathematical models based on physical principles have become essential tools for SOFC system design and analysis. While several SOFC models have been developed by different groups using different modeling assumptions, little analysis of the effects of these assumptions on model performance can be found in literature. Meanwhile, to support system optimization and control design activities, a trade-off often has to be made between high fidelity and low complexity. This trade-off can be influenced by the number of temperature layers assumed in the energy balance to represent the SOFC structure. In this paper, we investigate the impact of the temperature layer assumption on the performance of the dynamic planar SOFC model. Four models of co-flow planar SOFCs are derived using the finite volume discretization approach along with different assumptions in the number of temperature layers. The model with four temperature layers is used as the baseline model, and the other models aimed at reducing the complexity of the baseline model are developed and compared through simulations as well as linear analysis. We show that the model with as few as two temperature layers—the solid structure and air bulk flow—is able to capture the dynamics of SOFCs, while assuming only one temperature layer results in significantly large modeling error. [DOI: 10.1115/1.2971055]

1 Introduction

Given their high efficiency, low emissions, and flexible fueling options, solid oxide fuel cells (SOFCs) have great potential in many applications including stationary power plants and mobile auxiliary power unit systems [1]. Among different SOFC configurations, planar SOFCs have received increasing attention recently due to their compact size and higher power density and efficiency.

As SOFC technology evolves, mathematical models that can accurately describe steady-state and dynamic behaviors of SOFCs have become critical tools for SOFC system design and evaluation. Several dynamic models have been reported for planar SOFCs in the literature [2–9] and used to investigate their dynamics. Transient operating issues such as slow load following and large overshoots of temperature and temperature gradient have been identified in the dynamic response of SOFC systems [8,10–12], necessitating feedback control strategies to improve the system transient performance. In order to facilitate model-based control design and analysis, a simplified dynamic model with a low order that preserves the key dynamic characteristics of the system is always desirable.

Among the planar SOFC dynamic models reported in the literature, it has been recognized that different modeling assumptions have been used by different groups, thereby leading to different levels of model accuracy and complexity. For instance, different assumptions of temperature layers to represent the temperature distribution along the axis perpendicular to the cell plate have been used in these models, resulting in different numbers of temperature states in the energy balance dynamics of the fuel cell. Table 1 summarizes the different temperature layer assumptions found in the literature for dynamic planar SOFC modeling. Five temperature layers, i.e., fuel bulk flow, air bulk flow, positive electrode–electrolyte–negative electrode (PEN) assembly, and fuel/air-side interconnectors, are assumed in the SOFC models developed in Refs. [3,8]. In Refs. [5,6], four temperature layers are used by considering the fuel and air-side interconnectors as one part for the cells in the middle of the SOFC stack. A three-temperature-layer assumption can be found in the models derived in Refs. [2,4], where the PEN and interconnector are combined as one temperature layer, called solid structure. In Refs. [7,9], only one temperature layer is assumed.

By combining layers with similar steady-state and dynamic characteristics in temperature response, the energy balance dynamics in the SOFC model can be simplified and the number of temperature states in the model is minimized. This model reduction, however, is only possible if the consequences of the simplification can be fully understood and the trade-off between model accuracy and complexity thoroughly evaluated. However, limited analysis has been reported about the influence of the temperature layer assumption on the performance of the dynamic planar SOFC model. Campanari et al. compared steady-state planar SOFC models with three (fuel, air, and solid structure) and nine (fuel, air, PEN, three in fuel-side interconnector, and three in air-side interconnector) temperature layers in Ref. [13], based on steady-state simulation results. More recently, we studied the dynamic responses of planar SOFC models with assumptions of one to four temperature layers [14].

This paper extends the analysis presented in the conference paper [14]. A dynamic baseline model of the co-flow planar SOFC is first derived. Given the scope of this study, the description is focused on the energy balance part. Finite volume discretization approach is applied to capture the spatial distribution of variables inside the fuel cell. In this baseline model, four temperature layers, i.e., fuel bulk flow, air bulk flow, PEN, and interconnector, are assumed, introducing four temperature states in the energy balance dynamics for each discretization unit. Three different assumptions with reduced numbers of temperature layers are then proposed for model simplification. The effects of these modeling

[1]Corresponding author.

Manuscript received May 3, 2007; final manuscript received November 26, 2007; published online November 6, 2008. Review conducted by Umberto Desideri.

Table 1 Different modeling assumptions of temperature layers found in literature

Ref.	Assumption of temperature layers
[3,8]	Five temperature layers: fuel bulk flow air bulk flow PEN fuel-side interconnector air-side interconnector
[5,6]	Four temperature layers fuel bulk flow air bulk flow PEN interconnector
[2,4]	Three temperature layers: fuel bulk flow air bulk flow solid structure
[7,9]	One temperature layer: solid structure

assumptions on the performance of the dynamic planar SOFC model are evaluated by comparing both steady-state and transient simulations as well as performing linear analysis. As the endothermal direct internal reforming (DIR) activity in the SOFC could have a strong influence on the dynamics of the fuel cell, the impact of DIR on the selection of the temperature layer assumption is also investigated.

The rest of this paper is organized as follows: a dynamic baseline model is first described for a co-flow planar SOFC. Different assumptions of temperature layers for the SOFC modeling are then proposed and compared to evaluate the impact of the temperature layer assumption on the model performance. Conclusions and future work are discussed at the end of this paper.

2 Baseline Model of Co-flow Planar SOFCS

Figure 1 illustrates the operating principle of the co-flow planar SOFC considered in this paper. Six species, namely, CH_4, CO, CO_2, H_2O, H_2, and N_2, are assumed in the fuel stream, and the fuel inlet composition depends on the type and operation condition of the fuel reformer. Dry air is fed into the cathode of the fuel cell as oxidant and coolant. As shown in Fig. 1, besides the electrochemical reactions, the steam reforming (SR) and water gas shift (WGS) reactions in the fuel bulk flow are considered. Thus, all the reactions incorporated in the SOFC model are listed as follows:

- SR: $CH_4+H_2O \rightarrow CO+3H_2$
- WGS: $CO+H_2O \leftrightarrow CO_2+H_2$
- Oxidation (ox): $H_2+O^{2-} \rightarrow H_2O+2e^-$
- Reduction (red): $0.5O_2+2e^- \rightarrow O^{2-}$.

The planar SOFC is often considered as a distributed parameter system in order to capture the spatial distribution along the flow field for variables such as temperature, species concentration, and current density [2–6,8,15]. The governing equations are described using either partial differential equations or discretization technique. In this paper, the finite-volume discretization approach [8,13,16,17] is applied to derive the model for the co-flow planar SOFC shown in Fig. 1. Using this method, the cell is virtually divided into a user-defined number of small units along the bulk flow direction, as illustrated in Fig. 2, where the electrode and electrolyte layers are considered as one assembly structure, called the PEN. These discretization units are integrated to form the SOFC model by imposing the gas flows, heat exchanges, and current distribution relations.

Because of the high electrical conductivities of the interconnectors, the cell is assumed equipotential among the discretization units, and therefore we have

$$U^j = U_{\text{cell}}, \quad j = 1,2,\ldots,J \tag{1}$$

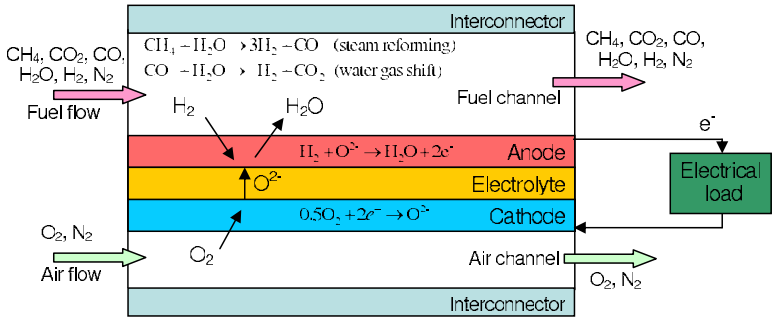

Fig. 1 Co-flow planar SOFCs (dimensions of the layers are not to scale)

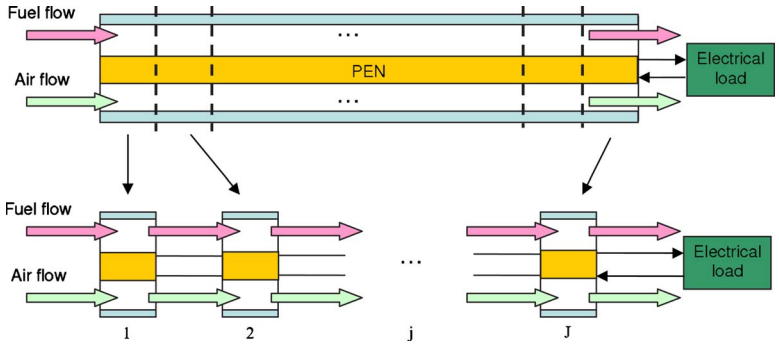

Fig. 2 Finite volume discretization for co-flow planar SOFCs

$$\sum_{j=1}^{J} i^j A^j = I \tag{2}$$

where U^j and U_{cell} are the operating voltages of the jth unit and the entire cell, respectively, J is the total number of the discretization units, i^j and A^j are the current density and the electrochemical reaction area, respectively, in the jth unit, and I is the total current drawn from the cell. U^j can be calculated as follows:

$$U^j = U^j_{\text{OCV}} - \eta^j, \quad j = 1,2, \ldots J \tag{3}$$

where U^j_{OCV} is the open circuit voltage in the jth unit and can be determined by the Nernst equation [1,18]. η^j represents the total potential loss due to various sources, including the internal resistance, activation energy, and gas species diffusion. Equation (3) defines the polarization relation in the jth discretization unit in the SOFC, where U^j is a function of local gas flow concentration, pressure, cell temperature, as well as current density. Detailed description of the approach for calculating U^j_{OCV} and η^j in Eq. (3) can be found in Ref. [19]. and is omitted here to avoid duplication.

For the jth discretization unit, the following are defined:

- n^j_{in,s_f} and n^j_{out,s_f}, $s_f \in \{\text{CH}_4, \text{CO}_2, \text{CO}, \text{H}_2\text{O}, \text{H}_2, \text{N}_2\}$: the inlet and outlet molar flux of species s_f in the fuel bulk flow, respectively
- n^j_{in,s_a} and n^j_{out,s_a}, $s_a \in \{\text{O}_2, \text{N}_2\}$: the inlet and outlet molar flux of species s_a in the air bulk flow, respectively
- $q^j_{\text{in},f}$ and $q^j_{\text{out},f}$: the inlet and outlet enthalpy flux in the fuel bulk flow, respectively
- $q^j_{\text{in},a}$ and $q^j_{\text{out},a}$: the inlet and outlet enthalpy flux in the fuel bulk flow, respectively

From the mass and energy conservation in bulk flows, we have

$$n^j_{\text{in},s_f} = n^{j-1}_{\text{out},s_f} \tag{4}$$

$$n^j_{\text{in},s_a} = n^{j-1}_{\text{out},s_a} \tag{5}$$

$$q^j_{\text{in},f} = q^{j-1}_{\text{out},f} \tag{6}$$

$$q^j_{\text{in},a} = q^{j-1}_{\text{out},a}$$

$$j = 2, \ldots, J \tag{7}$$

The boundary conditions, n^1_{in,s_f}, n^1_{in,s_a}, $q^1_{\text{in},f}$ and $q^1_{\text{in},a}$, depend on the fuel and air inlets to the fuel cell. The outlet molar and enthalpy flux in the fuel and air channels of each discretization unit can be calculated as follows:

$$n^j_{\text{out},s_f} = u^j_{\text{out},f} C^j_{s_f} \tag{8}$$

$$n^j_{\text{out},s_a} = u^j_{\text{out},a} C^j_{s_a} \tag{9}$$

$$q^j_{\text{out},f} = u^j_{\text{out},f} \sum_{s_f} C^j_{s_f} h_{s_f}(T^j_f) \tag{10}$$

$$q^j_{\text{out},a} = u^j_{\text{out},a} \sum_{s_a} C^j_{s_a} h_{s_a}(T^j_a)$$

$$j = 1, \ldots, J \tag{11}$$

where $u^j_{\text{out},f}$ and $u^j_{\text{out},a}$ are the speeds of the fuel and air outlet flows in the jth unit, respectively. $C^j_{s_f}$ and $C^j_{s_a}$ are the species concentrations in the fuel and air bulk flows, respectively. $h_s(T)$ is the specific enthalpy of species s at temperature of T. Given the small pressure drop across the fuel cell, $u^j_{\text{out},f}$ and $u^j_{\text{out},a}$ can be obtained using linear orifice relations and ideal gas law [8]. The species concentrations, $C^j_{s_f}$ and $C^j_{s_a}$, are determined by the mass balance dynamics, and the fuel and air temperature, T^j_f and T^j_a, by the energy balance.

2.1 Mass Balance Dynamics. The mass balance dynamics of gas species in the fuel and air bulk flows in the jth discretization unit can be described as follows:

$$\text{fuel:} \quad \dot{C}_{s_f} = (n_{\text{in},s_f} - n_{\text{out},s_f}) \frac{1}{l} + \sum_{k \in \{\text{SR,WGS,ox}\}} \nu_{s_f,k} r_k \frac{1}{d_f}$$

$$s_f \in \{\text{CH}_4, C\text{O}_2, \text{CO}, \text{H}_2\text{O}, \text{H}_2, \text{N}_2\} \tag{12}$$

$$\text{air:} \quad \dot{C}_{s_a} = (n_{\text{in},s_a} - n_{\text{out},s_a}) \frac{1}{l} + \nu_{s_a,\text{red}} r_{\text{red}} \frac{1}{d_a}$$

$$s_a \in \{\text{O}_2, \text{N}_2\} \tag{13}$$

where the superscript j of all the variables is omitted because they all refer to the same discretization unit. This notation simplification will also be applied to other equations in the rest of this paper, due to the same reason. In Eqs. (12) and (13), l is the length of the discretization unit, $\nu_{\cdot,k}$ is the stoichiometric coefficient in reaction k, r_k is the kinetic rate of reaction k, and d_f and d_a are the heights of the fuel and air channel, respectively. The reaction rates, r_k, are calculated following the approach used in Ref. [19].

2.2 Energy Balance Dynamics. As mentioned in Sec. 1, one or more temperature layers are usually assumed in SOFC modeling to describe the temperature variation in the axis normal to the cell plate. Due to their small thickness and tight connection, the three layers in the PEN structure are often assumed to have the same temperature in dynamic SOFC models [2–9]. In the SOFC model developed in Ref. [8], five temperature layers, i.e., PEN, fuel/air bulk flows, and fuel/air-side interconnectors are assumed. Note that, in the middle of a planar SOFC stack, the fuel/air-side interconnectors of adjoining cells are either manufactured as one part or tightly packaged together. The fuel/air-side interconnectors of adjacent cells can be treated as one temperature layer, called the interconnector, to reflect this assembly structure in the middle of the stack. Since the model developed here is intended to describe the cell in the middle of a co-flow planar SOFC stack, we consider four temperature layers, i.e., the fuel bulk flow, air bulk flow, PEN, and interconnector, in each discretization unit of the baseline SOFC model.

The temperatures in these four layers are calculated by solving the dynamic energy balance in each layer. The heat transfer considered in the model includes the convection between the bulk flows and their surrounding solid structures, the conduction in solid layers as well as radiation between PEN and interconnectors.

The energy balance dynamics in the fuel flow can be expressed as follows:

$$\frac{d}{dt}\left(\sum_{s_f} C_{s_f} e_{s_f}\right) = (q_{\text{in},f} - q_{\text{out},f}) \frac{1}{l} + [k_{f,\text{PEN}}(T_{\text{PEN}} - T_f) + k_{f,I}(T_I - T_f)] \frac{1}{d_f} + r_{\text{ox}}[h_{\text{H}_2\text{O}}(T_{\text{PEN}}) - h_{\text{H}_2}(T_f)] \frac{1}{d_f} \tag{14}$$

where e_{s_f} is the specific internal energy of species s_f. The first term on the right hand side of Eq. (14) is due to the enthalpy flux of the bulk flow, and the second term accounts for the convective heat exchange between the fuel flow and its surrounding solid layers. The heat transfer coefficient can be obtained by assuming a constant Nusselt number of 4 [20]. The last term of Eq. (14) is caused by the enthalpy flux due to the ox reaction at the anode.

According to the relation for the ideal gas flow, $e_{s_f} = h_{s_f} - p_{s_f}/C_{s_f}$, where h_{s_f} is the specific enthalpy of species s_f, we can obtain

Table 2 Geometry parameters in SOFC model

Symbol	Definition	Unit	Value
J	Total number of discretization units		16
L	Cell length	m	0.4
W	Cell width	m	0.1
d_a	Air channel height	m	0.001
d_f	Fuel channel height	m	0.001
l	Length of discretization unit	m	$L/J=0.025$
τ_I	Thickness of interconnector	m	0.001
τ_{PEN}	Thickness of PEN	μm	570

$$\dot{T}_f = \frac{1}{\Sigma_{s_f} c_{v,s_f} C_{s_f}} \left\{ -\sum_{s_f} (h_{s_f}(T_f) - \tilde{R}T_f)\dot{C}_{s_f} + (q_{\text{in},f} - q_{\text{out},f})\frac{1}{l} + [k_{f,\text{PEN}}(T_{\text{PEN}} - T_f) + k_{f,I}(T_I - T_f)]\frac{1}{d_f} + r_{\text{ox}}[h_{\text{H}_2\text{O}}(T_{\text{PEN}}) - h_{\text{H}_2}(T_f)]\frac{1}{d_f} \right\} \quad (15)$$

Similarly, for the air flow, we have

$$\dot{T}_a = \frac{1}{\Sigma_{s_a} c_{v,s_a} C_{s_a}} \left\{ -\sum_{s_a} (h_{s_a}(T_a) - \tilde{R}T_a)\dot{C}_{s_a} + (q_{\text{in},a} - q_{\text{out},a})\frac{1}{l} + [k_{a,\text{PEN}}(T_{\text{PEN}} - T_a) + k_{a,I}(T_I - T_a)]\frac{1}{d_a} - 0.5 r_{\text{red}} h_{\text{O}_2}(T_a)\frac{1}{d_a} \right\} \quad (16)$$

From the energy balance in the solid components in the SOFC, the temperature dynamics in the PEN assembly and interconnector can be described as follows:

$$\dot{T}_{\text{PEN}} = \frac{1}{\rho_{\text{PEN}} c_{p,\text{PEN}}} \left\{ q_{\text{cond,PEN}}\frac{1}{l} - [k_{f,\text{PEN}}(T_{\text{PEN}} - T_f) + k_{a,\text{PEN}}(T_{\text{PEN}} - T_a)]\frac{1}{\tau_{\text{PEN}}} + r_{\text{ox}}[h_{\text{H}_2}(T_f) + 0.5 h_{\text{O}_2}(T_a) - h_{\text{H}_2\text{O}}(T_{\text{PEN}})]\frac{1}{\tau_{\text{PEN}}} - iU\frac{1}{\tau_{\text{PEN}}} + \frac{2\sigma(T_I^4 - T_{\text{PEN}}^4)}{1/\epsilon_I + 1/\epsilon_{\text{PEN}} - 1} \cdot \frac{1}{\tau_{\text{PEN}}} \right\} \quad (17)$$

$$\dot{T}_I = \frac{1}{\rho_I c_{p,I}} \left\{ q_{\text{cond},I}\frac{1}{l} - k_{f,I}(T_I - T_f)\frac{1}{\tau_I} - k_{a,I}(T_I - T_a)\frac{1}{\tau_I} - \frac{2\sigma(T_I^4 - T_{\text{PEN}}^4)}{1/\epsilon_I + 1/\epsilon_{\text{PEN}} - 1} \cdot \frac{1}{\tau_I} \right\} \quad (18)$$

where q_{cond} is the flux of heat conduction in the solid layers. The last terms in Eq. (17) and (18) are due to the radiation between the PEN and the interconnector.

The dimension and material properties given in Ref. [5] for an intermediate-temperature anode-supported planar SOFC are used in this paper for simulation and analysis. For the convenience of reference, some geometry parameters are listed in Table 2. A discretization grid with 16 evenly distributed units is selected here as a reasonable trade-off between model accuracy and simulation efficiency [8].

3 Analysis on Models With Different Assumptions of Temperature Layers

As shown in Table 1, different assumptions of temperature layers have been used in SOFC models developed by different researchers, leading to models with different complexities. In this section, the impacts of different temperature layer assumptions on the performance of the SOFC model are evaluated based on simulation results.

Table 3 Models with different assumptions of temperature layers

Model name	Assumption of temperature layers
4T (baseline model)	Four layers: fuel (T_f) air (T_a) PEN (T_{PEN}) interconnector (T_I)
3T	Three layers: fuel (T_f) air (T_a) solid structure (T_{sol}) $T_{\text{PEN}}=T_I=T_{\text{sol}}$
2T	Two layers: air (T_a) solid structure (T_{sol}) $T_f=T_{\text{PEN}}=T_I=T_{\text{sol}}$ neglect energy of the gas accumulated in the fuel channel
1T	One layer: solid structure (T_{sol}) $T_f=T_a=T_{\text{PEN}}=T_I=T_{\text{sol}}$ neglect energy of the gas accumulated in the fuel and air channels

3.1 Model Assumptions With Reduced Number of Temperature Layers. In Sec. 2, four temperature layers, namely, fuel bulk flow (T_f^j), air bulk flow (T_a^j), PEN (T_{PEN}^j), and interconnector (T_I^j), are assumed in the energy balance dynamics, introducing four temperature states to each discretization unit in the SOFC model. Given that our ultimate goal is to provide a dynamic model with low complexity for feedback control design and system optimization, we attempt to minimize the number of temperature layers in the model assumption, thereby reducing the number of temperature states, as long as the key dynamics of SOFC are preserved in the simplified model.

With the four-temperature-layer baseline model described in Sec. 2 also referred to as the 4T model), three other models with reduced numbers of temperature states can be constructed, as listed in Table 3.

- 3T: As the PEN assembly and the interconnector are the solid components in the fuel cell, the model called 3T considers them as one temperature layer with the same temperature profile and adopts the same assumption as used in Refs. [2,4]. In this model, three temperature layers, i.e., the fuel bulk flow, air bulk flow, and solid structure (consisting of PEN and interconnector) are assumed.
- 2T: One state is for the temperature of the air bulk flow and the other for the temperature of the remaining parts in each discretization unit. This model assumption can be justified by Fig. 3, where the open-loop temperature response of the baseline model at four different locations in the fuel cell, i.e., the temperature in the 1st (T^1), the 6th (T^6), the 11th (T^{11}), and the last (T^{16}) discretization units, are shown. During the simulation, the current load and gas inlet conditions of the SOFC system switch at 100 s from part load to full load setpoints that are listed in Table 4. These operating parameters are obtained through system steady-state optimization [12]. As can be seen from Fig. 3, the temperatures of the fuel bulk flow, PEN structure, and interconnector exhibit similar steady-state and dynamic responses, suggesting the possibility of combining these three parts as one tempera-

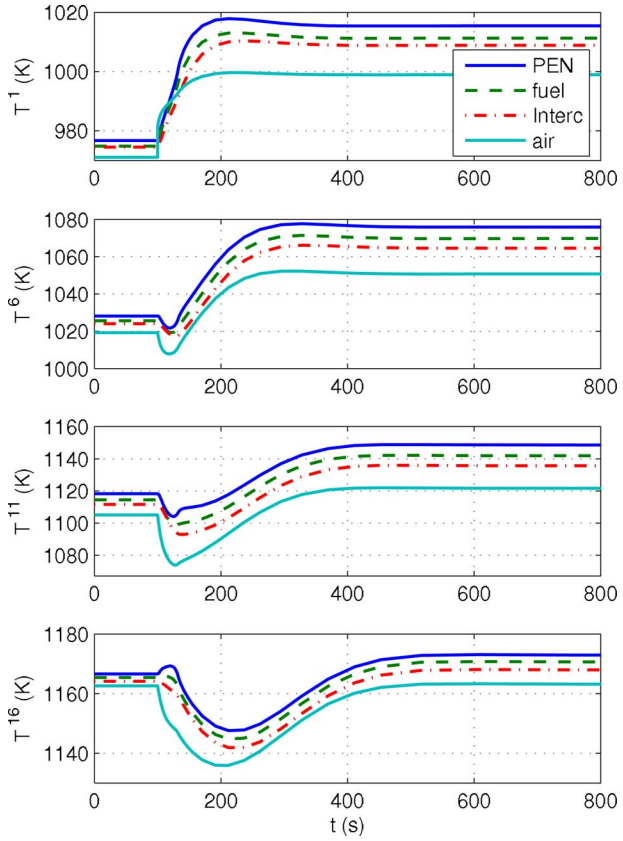

Fig. 3 Open-loop temperature response at different locations in the SOFC using the baseline 4T model

ture layer. In addition, considering the small volume in the gas channels, the energy of the gas accumulated in the fuel channel is neglected in the 2T assumption.

- 1T: Combining all four temperature layers into one gives the 1T model, where all layers in one discretization unit are assumed to have equal temperature and the energy of the gas accumulated in both fuel and air channels is neglected.

In order to isolate the effects of the reduced number of temperature states, except for the energy balance dynamics, other parts in the above three simplified models are kept the same as in the baseline 4T model.

While the governing equations of the temperature dynamics for the baseline model have been derived in Sec. 2, equations for other models are listed as follows (note again that the superscript j is omitted):

For 3T model: T_f, T_a, T_{sol},

Table 4 Operating parameters for the case with CPOX reformer

	Full load	Part load
Current load, I (A)	320	160
Ave. current density, $\bar{i}$ (A/cm^2)	0.8	0.4
Fuel utilization ratio	90%	90%
Oxygen/carbon ratio in CPOX	0.65	0.60
Inlet temperature of reformate to SOFC (K)	991	963
Air excess ratio	9.0	6.2
Inlet temperature of air to SOFC (K)	991	963

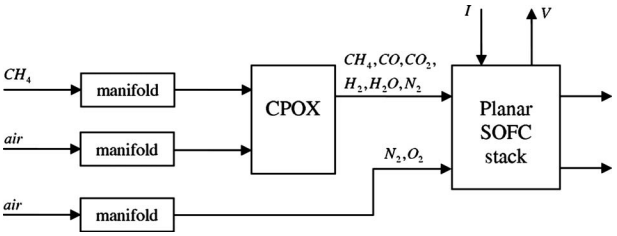

Fig. 4 Planar SOFC and CPOX system

$$\dot{T}_f = \frac{1}{\sum_{s_f} c_{v,s_f} C_{s_f}} \left\{ -\sum_{s_f} (h_{s_f}(T_f) - \tilde{R}T_f)\dot{C}_{s_f} + (q_{\text{in},f} - q_{\text{out},f})\frac{1}{l} + [k_{f,\text{PEN}}(T_{\text{sol}} - T_f) + k_{f,I}(T_{\text{sol}} - T_f)]\frac{1}{d_f} + r_{\text{ox}}[h_{\text{H}_2\text{O}}(T_{\text{sol}}) - h_{\text{H}_2}(T_f)]\frac{1}{d_f} \right\} \tag{19}$$

$$\dot{T}_a = \frac{1}{\sum_{s_a} c_{v,s_a} C_{s_a}} \left\{ -\sum_{s_a} (h_{s_a}(T_a) - \tilde{R}T_a)\dot{C}_{s_a} + (q_{\text{in},a} - q_{\text{out},a})\frac{1}{l} + [k_{a,\text{PEN}}(T_{\text{sol}} - T_a) + k_{a,I}(T_{\text{sol}} - T_a)]\frac{1}{d_a} - 0.5 r_{\text{red}} h_{\text{O}_2}(T_a)\frac{1}{d_a} \right\} \tag{20}$$

$$\dot{T}_{\text{sol}} = \frac{1}{\rho_{\text{PEN}} c_{p,\text{PEN}} \tau_{\text{PEN}} + \rho_I c_{p,I} \tau_I} \left\{ q_{\text{cond,PEN}}\frac{\tau_{\text{PEN}}}{l} + q_{\text{cond},I}\frac{\tau_I}{l} - k_{f,\text{PEN}}(T_{\text{sol}} - T_f) - k_{a,\text{PEN}}(T_{\text{sol}} - T_a) - k_{f,I}(T_{\text{sol}} - T_f) - k_{a,I}(T_{\text{sol}} - T_a) + r_{\text{ox}}[h_{\text{H}_2}(T_f) + 0.5 h_{\text{O}_2}(T_a) - h_{\text{H}_2\text{O}}(T_{\text{sol}})] - iU \right\} \tag{21}$$

For 2T model: T_a, T_{sol},

$$\dot{T}_a = \frac{1}{\sum_{s_a} c_{v,s_a} C_{s_a}} \left\{ -\sum_{s_a} (h_{s_a}(T_a) - \tilde{R}T_a)\dot{C}_{s_a} + (q_{\text{in},a} - q_{\text{out},a})\frac{1}{l} + [k_{a,\text{PEN}}(T_{\text{sol}} - T_a) + k_{a,I}(T_{\text{sol}} - T_a)]\frac{1}{d_a} - 0.5 r_{\text{red}} h_{\text{O}_2}(T_a)\frac{1}{d_a} \right\} \tag{22}$$

$$\dot{T}_{\text{sol}} = \frac{1}{\rho_{\text{PEN}} c_{p,\text{PEN}} \tau_{\text{PEN}} + \rho_I c_{p,I} \tau_I} \left\{ q_{\text{cond,PEN}}\frac{\tau_{\text{PEN}}}{l} + q_{\text{cond},I}\frac{\tau_I}{l} + (q_{\text{in},f} - q_{\text{out},f})\frac{d_f}{l} - k_{a,\text{PEN}}(T_{\text{sol}} - T_a) - k_{a,I}(T_{\text{sol}} - T_a) + 0.5 r_{\text{red}} h_{\text{O}_2}(T_a) - iU \right\} \tag{23}$$

For 1T model: T_{sol},

$$\dot{T}_{\text{sol}} = \frac{1}{\rho_{\text{PEN}} c_{p,\text{PEN}} \tau_{\text{PEN}} + \rho_I c_{p,I} \tau_I} \left\{ q_{\text{cond,PEN}}\frac{\tau_{\text{PEN}}}{l} + q_{\text{cond},I}\frac{\tau_I}{l} + (q_{\text{in},f} - q_{\text{out},f})\frac{d_f}{l} + (q_{\text{in},a} - q_{\text{out},a})\frac{d_a}{l} - iU \right\} \tag{24}$$

3.2 Model Performance Comparison. The performance of these SOFC models, which assumed different temperature layers, are first compared using the simulation platform developed in Ref. [12], where the SOFC system configuration illustrated in Fig. 4 is

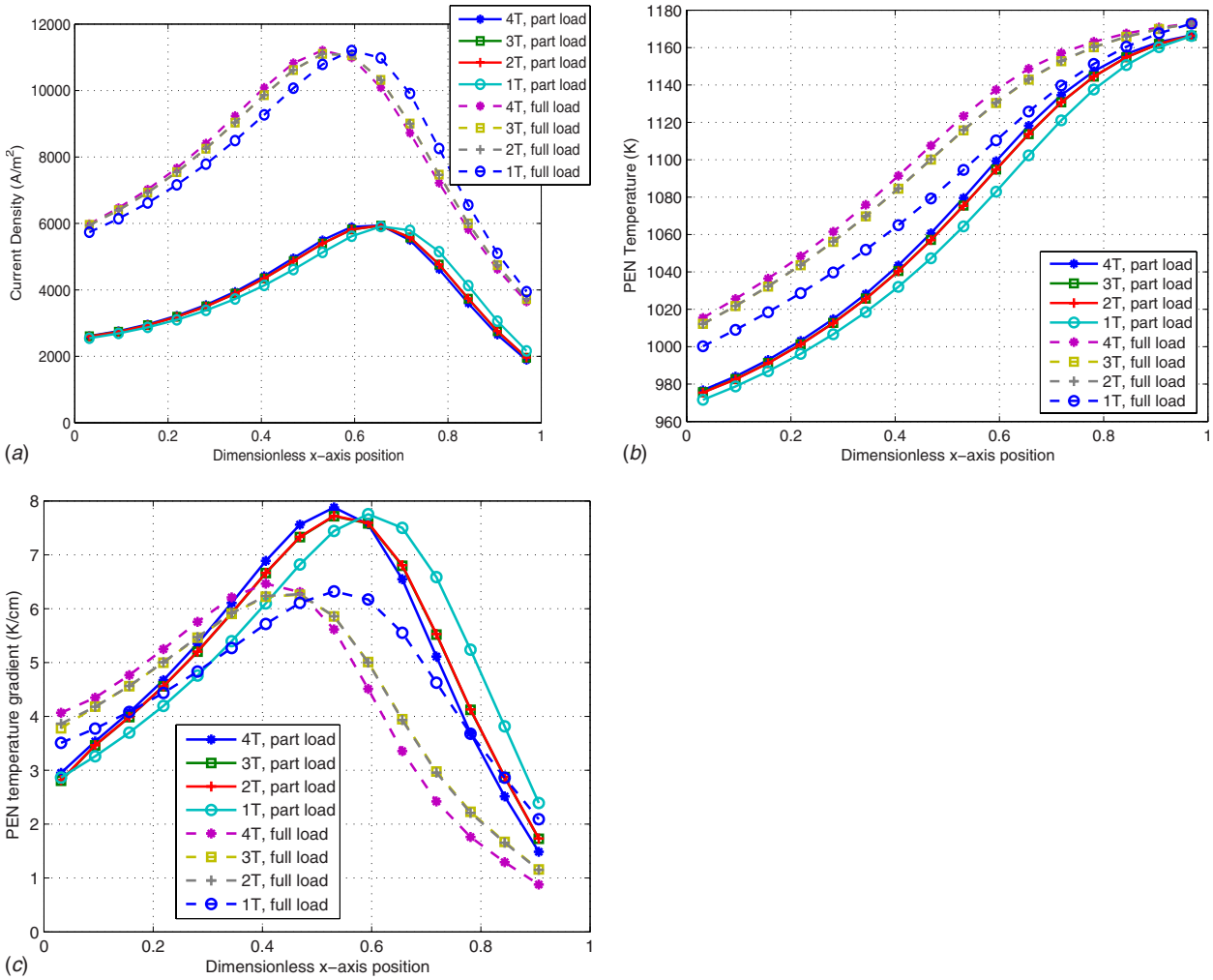

Fig. 5 Steady-state spatial distributions of (*a*) current density, (*b*) PEN temperature, and (*c*) temperature gradient

used. This system consists of a 25-cell co-flow planar SOFC stack, an external catalytic partial oxidation (CPOX) fuel processor and gas supply manifolds. Furthermore, in order to evaluate the impacts of the strongly endothermal SR reaction on the model simplification result, another case, where the fuel inlet to the SOFC contains a relatively high fraction of CH_4 and significant DIR activity takes place in the fuel cell, is also discussed at the end of this section.

3.2.1 Simulation Results and Linear Analysis. Figure 5 compares the steady-state spatial distributions of the current density, PEN temperature, and temperature gradient in the SOFC for both the part and full load operation conditions listed in Table 4. In Fig. 5, even though the four models exhibit similar trends in their distribution curves, noticeable degradation is shown in the 1T model, compared to the 2T and 3T models. In particular, the distributions of the PEN temperature and temperature gradient at full load operation show the largest error between the 1T and the baseline model. The larger modeling error shown at full load than at part load is due to the larger steady-state temperature difference between different layers at higher load level, as shown in Fig. 3. On the other hand, no significant difference between the 3T and 2T models at steady state can be observed.

Figure 6 provides a comparison of the open-loop dynamic response of different models to load increase and decrease. A 5 A/s rate limiter is applied to the current increase in order to avoid fuel starvation in the SOFC caused by the fuel supply delay [12]. One can see from Fig. 6 that, while the dynamic responses of the 3T

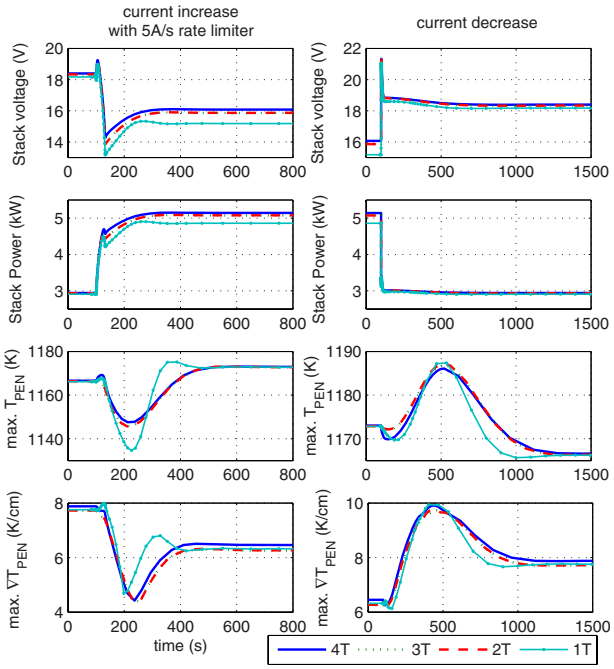

Fig. 6 Comparison of open-loop response with model assumptions in Table 3

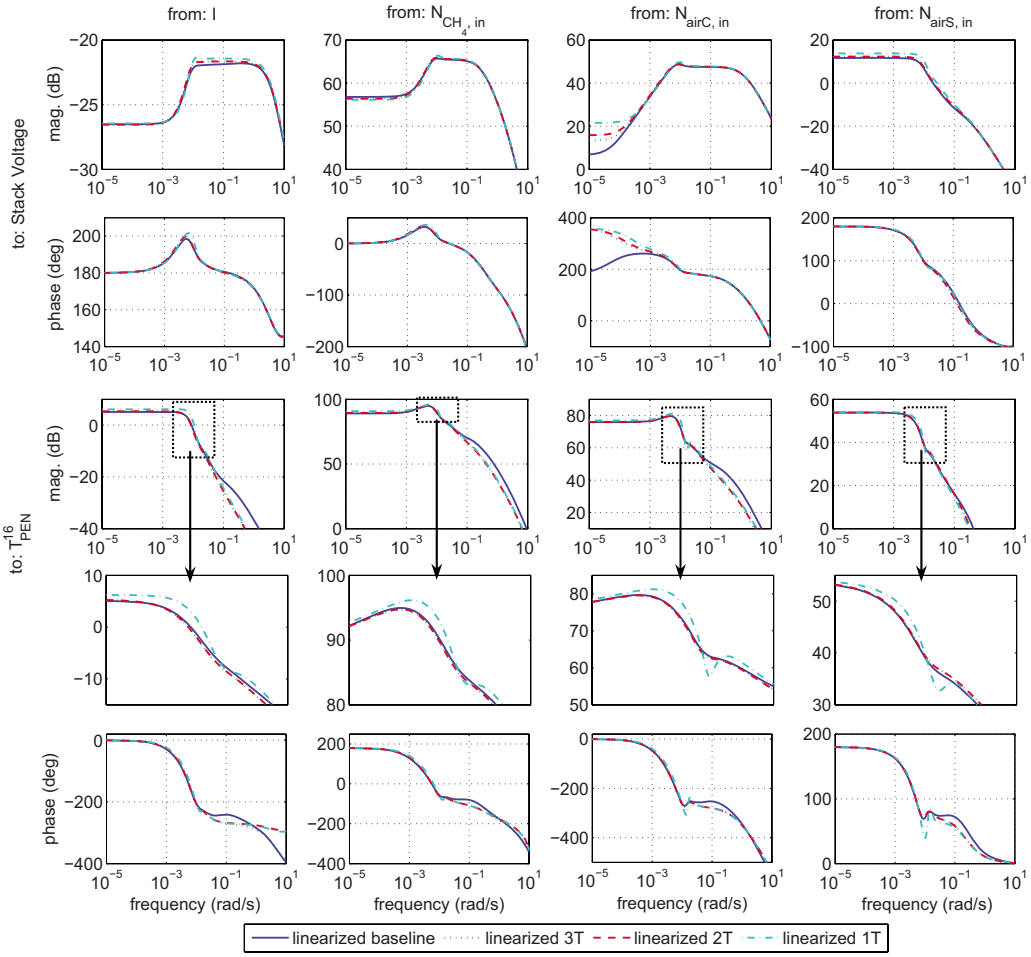

Fig. 7 Bode plots of linearized models at part load operation condition

and 2T models match the baseline model fairly well, the 1T model exhibits different transient behaviors for both the current increase and decrease cases, especially in the response of maximum temperature and temperature gradient in the PEN structure when the current load increases. The dynamic simulation results show almost identical transient response for the 3T and 2T models.

The observations obtained based on simulations can also be confirmed by linear analysis. Figures 7 and 8 show the bode plots [21] of the linearized models at the part and full load operation conditions, respectively. In these plots, we show the frequency response of the stack voltage and maximum PEN temperature (T^{16}_{PEN}) to the system inputs, which include the total current (I) and gas supply flow rates of CH_4 ($N_{CH_4,in}$), air to the CPOX ($N_{airC,in}$), and air to the cathode ($N_{airS,in}$). As shown in Figs. 7 and 8, the linearized 1T model exhibits larger modeling error in the frequency response of T^{16}_{PEN}, compared to the 3T and 2T models. For example, as shown in Fig. 8, the 1T model has a higher bandwidth than the other models in the response of T^{16}_{PEN} to $N_{airS,in}$. In addition, the decaying rate of the magnitude is much faster in the 1T model than the other models at the frequency about 0.01–0.1 rad/s, suggesting that the 1T model has higher order dynamics that do not exist in the other models. This is also consistent with the simulation results shown in Fig. 9, which compares the transient response of the maximum PEN temperature, T^{16}_{PEN} in the co-flow SOFC, for different models subject to a 5% perturbation in $N_{airS,in}$ at the full operation condition. One can see that the 2T and 4T models have similar dynamic behaviors, which can be approximated by a first-order dynamic system. The 1T model, however, exhibits quite different dynamics that correlate with the higher order system response. From Figs. 7 and 8, it can also be found that the linearized 3T and 2T models have almost the same frequency response shown in these bode plots.

From Fig. 7, it is noted that the dc gain in the stack voltage response to $N_{airC,in}$ has different signs for the simplified models and the baseline model at the part load operation condition. This is due to the system nonlinearity as well as the modeling error caused by combining the PEN and interconnector as one temperature layer at this particular operating setpoint. Figure 10 compares the sensitivity of the steady-state stack voltage to small perturbations in $N_{airC,in}$ for the 4T and 3T models at the part load operation condition. It can be found that, although the two curves exhibit similar trend in general, they have slopes with different signs at the operation point, which accounts for the different sign of the dc gains in the linear analysis. Despite this difference of the dc gains in linear analysis, the dynamic behavior of the 3T model is close to that of the 4T model, as shown in Fig. 11 where the system is subject to 0.1% and 1% perturbations in $N_{airC,in}$. From Fig. 11, one can observe that the transient response of different models have similar characteristics. However, for the 0.1% perturbation case, the 4T model predicts a steady-state voltage decrease while the 3T model predicts an increase, which is consistent with the linear analysis results. Both models show steady-state voltage decrease when the perturbation is increased to 1%. Due to the small sensitivity of the voltage to $N_{airC,in}$, this subtle difference does not result in noticeable modeling error when the 4T model is reduced to the 3T and 2T models.

3.2.2 Reason for the Modeling Error in the 1T Model. The

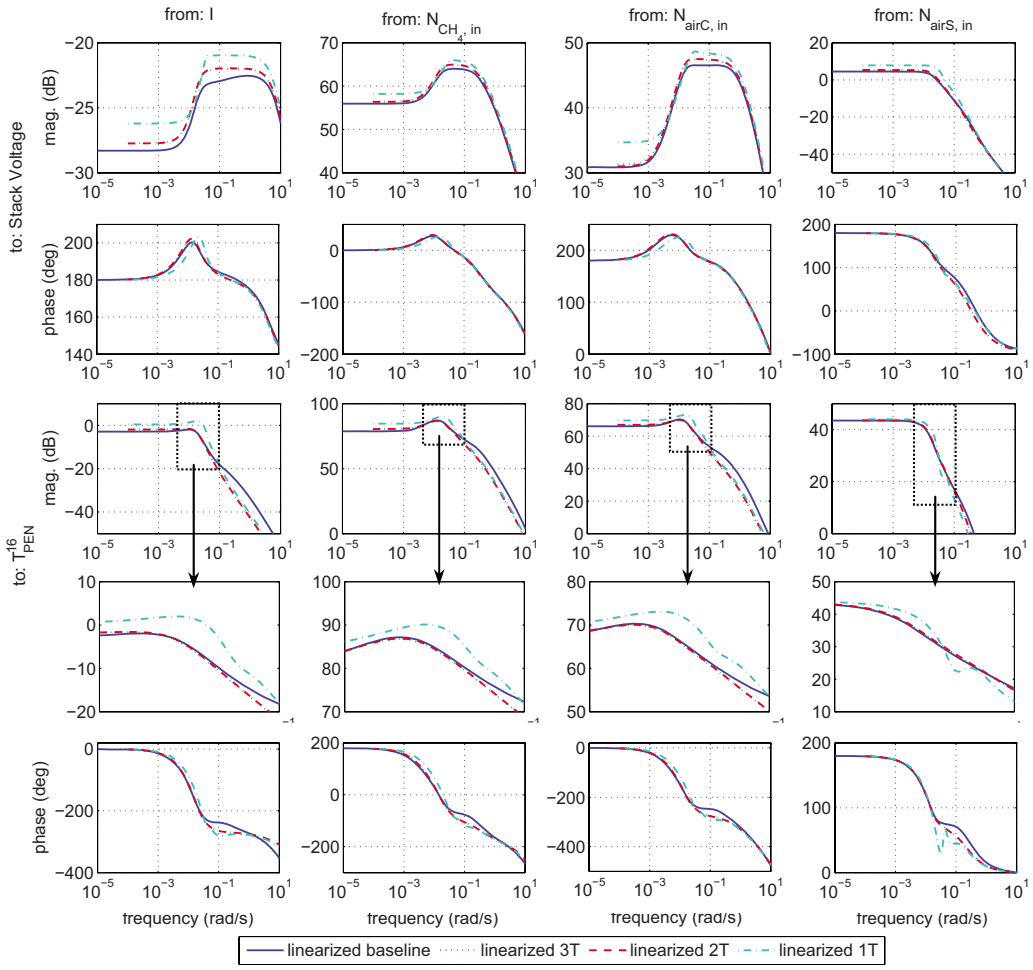

Fig. 8 Bode plots of linearized models at full load operation condition

large model error resulting from the 1T assumption arises, in part, because this assumption implies an infinite heat transfer rate between the air bulk flow and its surrounding solid structure. However, due to the relatively high velocity of the air flow and the limited heat transfer rate, the air flow and solid structure are not able to sufficiently exchange energy to reach the same temperature (refer to Fig. 3). To illustrate this effect, we constructed an artificial SOFC model with increased convective heat transfer coefficients (two times and ten times of actual one) between the air bulk flow and the solid structure, and show the simulation results in Fig. 12. For comparison, the responses of the 4T model with original heat transfer coefficients and the 1T model are also plotted. From Fig. 12, as the heat transfer rate between the air flow and the solid walls increases, the response of the baseline 4T model becomes closer to that of the 1T model, verifying our hypothesis regarding the source of the model error introduced by the 1T

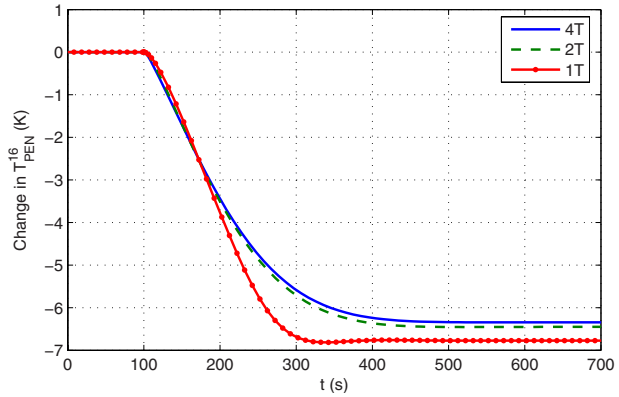

Fig. 9 Dynamic response of T^{16}_{PEN} to a 5% step increase of $N_{airS,in}$ at the full load operation setpoint

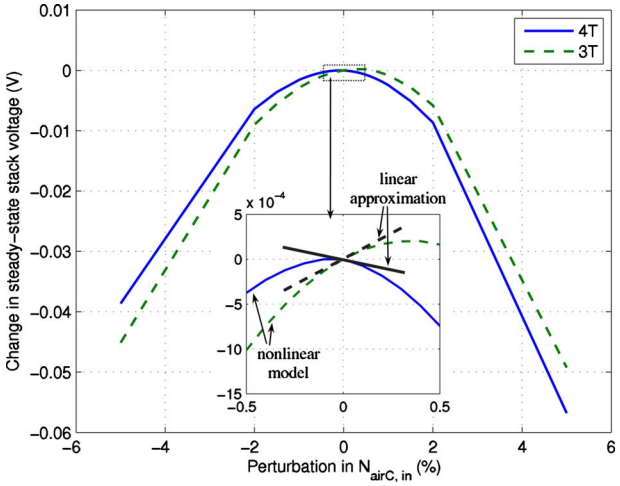

Fig. 10 Steady-state response of stack voltage to small perturbation in $N_{airC,in}$ around part load operation condition

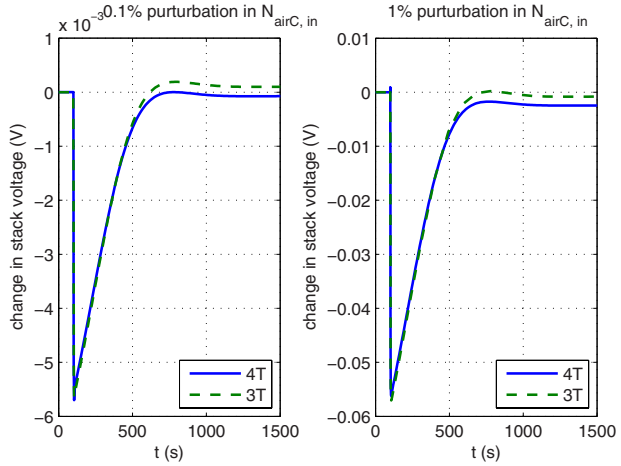

Fig. 11 Dynamic response of stack voltage to small perturbation in $N_{airC,in}$ around part load operation condition

assumption. The relatively larger model error observed in the case of current increase shown in Fig. 6 can also be explained since the model error caused by the 1T assumption becomes more significant with faster air flow velocity at high load.

Compared to the air flow, the fuel flow has much lower velocity. For example, at the part load operation condition given in Table 4, the fuel flow velocity is about 1.5 m/s and the air flow about 10.5 m/s. The difference between the fuel and air flow speeds is even larger at full load operation (about 3.3 m/s versus about 30 m/s) because of the higher air excess ratio used at full load operation. At these speeds, the fuel flow can conduct sufficient heat transfer with the solid structure, resulting in a similar temperature response in the fuel flow and solid parts, as shown in Fig. 3. Therefore, combining the fuel bulk flow and solid structure into one temperature layer, as in the 2T model, does not introduce significant error for our system. Figure 13 compares simulation results when the heat transfer coefficient between the fuel flow and the solid structure is intentionally decreased (5% and 0.5% of actual one) in the baseline model. As this heat transfer coefficient decreases, the 2T assumption would cause a larger model error, especially in the dynamic response of the maximum PEN temperature.

3.2.3 Effects of Low Fuel Utilization and Fast Current Increase. Figure 14 shows the simulation results of the system with the same operating parameters in Table 4, except that a lower fuel utilization ratio (50%) is used. The rate limiter of current increase is set at 20 A/s in this case to allow a more rapid increase in the current load during transient. While the 1T model

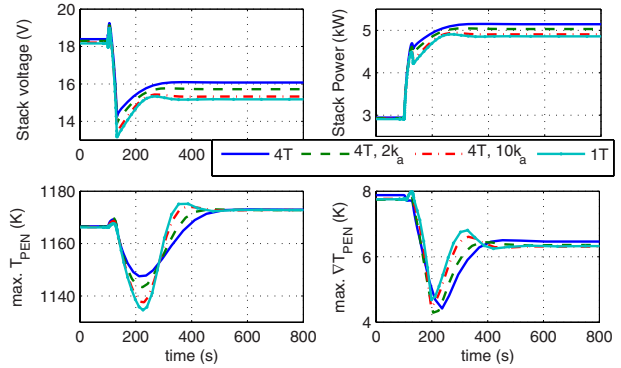

Fig. 12 Effects of heat transfer rates between air flow and solid structure on open-loop response to load increase

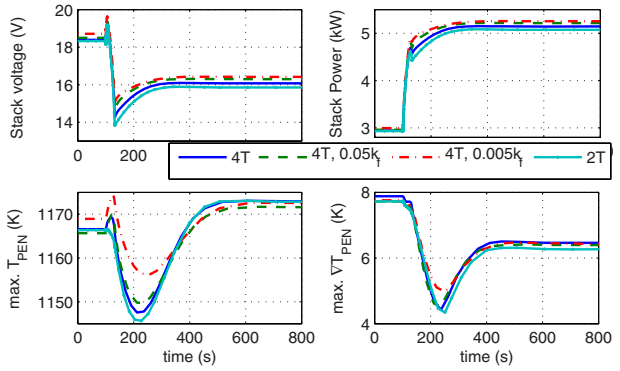

Fig. 13 Effects of heat transfer rates between fuel flow and solid structure on open-loop response to load increase

leads to significant model error, the 2T and 3T models are still consistent with the baseline model in dynamic response, especially considering the trend in slow dynamics. Compared to the simulation results plotted in Fig. 6, larger differences in the response of the maximum PEN temperature can be observed between the 2T/3T and baseline models in Fig. 14 during the short period right after the current load is increased. This is because the lower fuel utilization ratios result in a higher current density in the last unit, which corresponds to the highest PEN temperature in the co-flow SOFC. With more rapid current increases, more heat is generated in the PEN structure of the last unit and accumulated here due to the finite, albeit fast, heat transfer rate between the PEN assembly and the other layers. Nevertheless, as shown in Fig. 14, the trend in the dynamic response of the 2T model still retains the main characteristics of the baseline model fairly well. Considering practical constraints such as actuator saturations and dynamics in parasitic devices, the current increase in the last unit during transients will be very limited in normal operations. Thus, the error introduced by combining the PEN and interconnector into one temperature layer can be expected to be negligible for our applications.

As revealed by the above analysis, the 2T assumption, i.e., as-

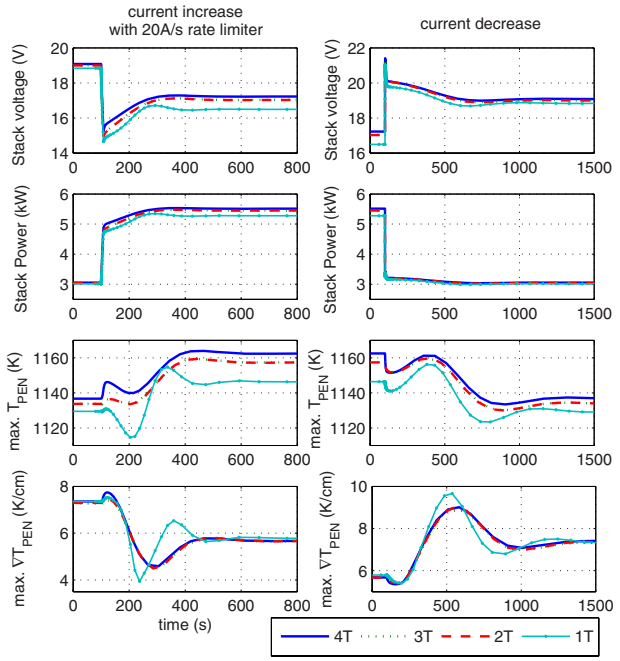

Fig. 14 Comparison of open-loop response with model assumptions in Table 3. Fuel utilization ratio=50%.

Table 5 Comparison of computation efficiency

Model	Number of states in each discretization unit	Number of states in SOFC model[a]	CPU time (s)
4T	12	192	522
3T	11	176	335
2T	10	160	316
1T	9	144	360

[a]Based on the 16-unit discretization scheme.

suming two temperature layers (the air bulk flow and the solid structure) in the energy balance, represents a good trade-off between model accuracy and complexity. In this simplification, two states in each discretization unit are removed from the baseline model while the key dynamic characteristics are preserved. This model simplification also results in a significant reduction in computation time, as shown in Table 5. All the models are built in MATLAB/SIMULINK. The CPU time reported is the average of three times the simulations considered in Fig. 6, with the current increase from part to full load. All simulations are run on a desktop with a Pentium4 3.2 GHz CPU and 504 Mbyte memory. As shown in Table 5, the 2T model can save about 40% CPU time, compared to the baseline model. It is also noted, however, that the 1T model imposes even more computation burden than the 3T and 2T ones do, and the reason needs to be investigated.

3.3 Impacts of Direct Internal Reforming on Performance of Simplified Model. Reforming methane through SR and WGS reactions inside the fuel channel of SOFCs, as shown in Fig. 1, is called DIR and has the potential to reduce the size of the external reformer and improve system efficiency [1]. As shown in Sec. 2, DIR has been incorporated in the baseline model. Note that SR is a strongly endothermal reaction ($\Delta H^0 = 206$ kJ/mol); DIR could have significant influence on the spatial distribution and dynamic response of the SOFC, and therefore its impacts on model simplification results need to be analyzed.

For SOFC systems fed with fuels processed by the CPOX reformer, however, the amount of CH_4 remaining in the reformate is relatively small (less than 2% in molar fraction for the operation conditions given in Table 4), which leads to insignificant steam reforming activity inside the SOFC. In order to investigate the effects of DIR on the performance of the SOFC models with simplified energy balance dynamics, it is assumed in the following that the fuel fed to the SOFC is reformed through an external SR pre-reformer with a specified pre-reforming ratio. The pre-reforming ratio is defined as the fraction of CH_4 processed in the reformer over the total amount of fuel entering the reformer. More CH_4 will remain in the reformate at lower pre-reforming ratio and reacts through the DIR inside the fuel channel of the SOFC.

Steady-state simulation results using models with different temperature layer assumptions in this case are compared in Fig. 15, while Fig. 16 compares dynamic responses of these models. The operation parameters listed in Table 6 are used, where the pre-

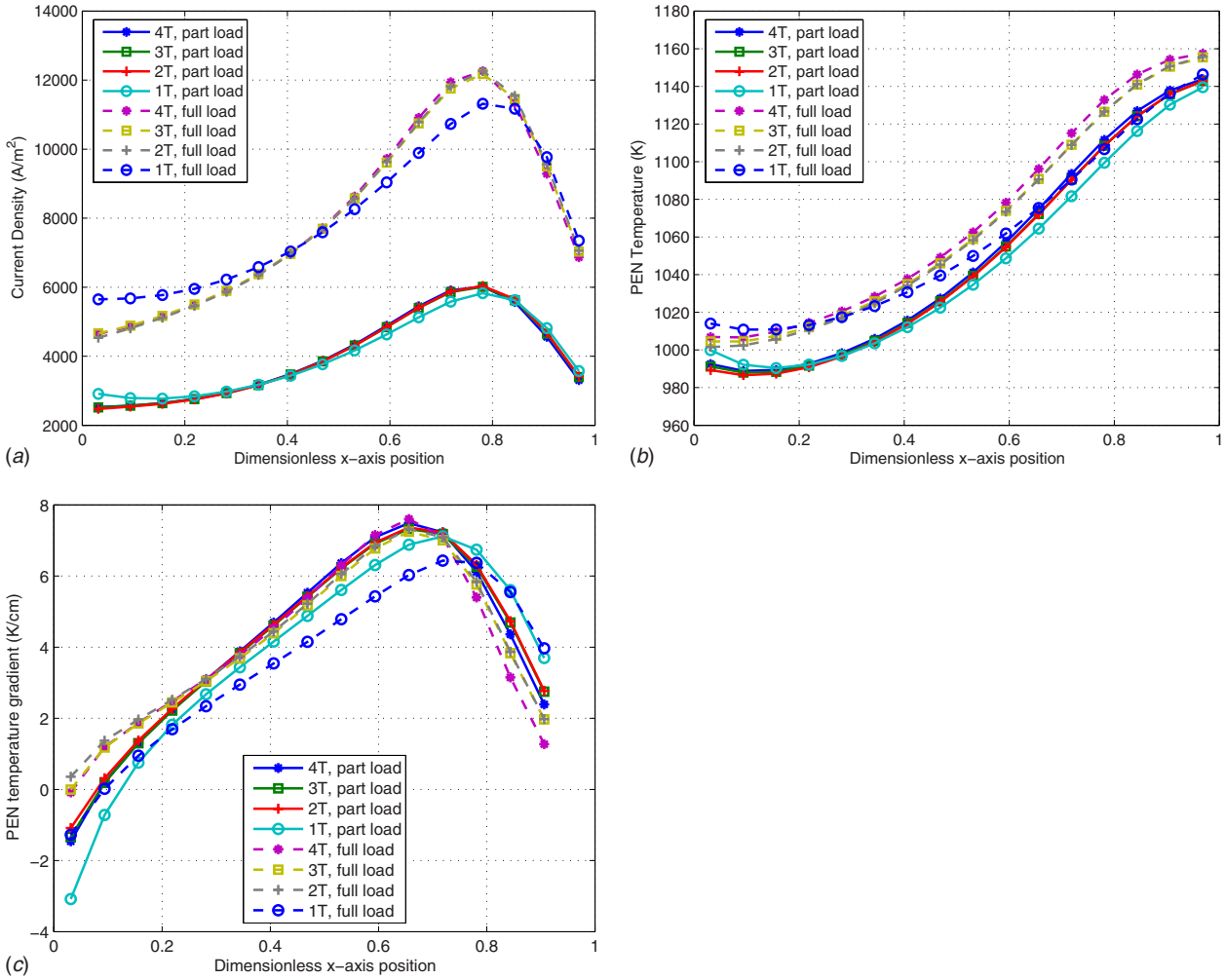

Fig. 15 Steady-state spatial distributions of (*a*) current density, (*b*) PEN temperature, and (*c*) temperature gradient. Operating setpoints given in Table 6 are used for simulations

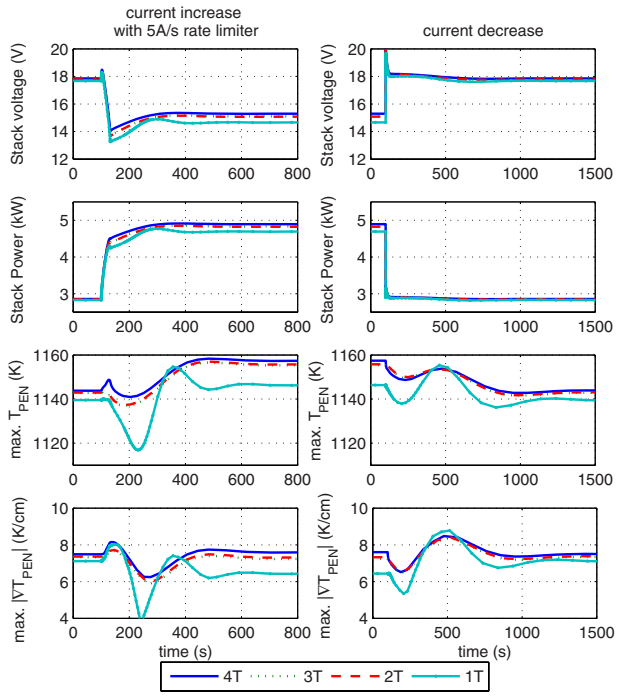

Fig. 16 Open-loop response with model assumptions in Table 3. Operating setpoints given in Table 6 are used for simulations.

reforming ratio in the SR fuel processor is set at 20%, i.e., 80% CH_4 supplied to the system remains unreformed before entering the SOFC, resulting in a 23.5% molar fraction of CH_4 in the fuel inlet to the fuel cell. From Figs. 15 and 16, the same conclusion can be drawn that the responses of the model with the 2T and 3T assumptions resemble the dynamic characteristics of the baseline model, while the 1T assumption induces large model errors. Therefore, DIR has insignificant influence on model simplification results for the system under consideration. The 2T model is valid even when substantial unreformed CH_4 is fed directly into the SOFC and reformed through DIR inside the fuel cell.

4 Conclusion and Future Work

Different assumptions of temperature layers result in different levels of accuracy and complexity in the SOFC models. In this paper, four models with different numbers of temperature layers are explored for co-flow planar SOFCs. The impacts of these different assumptions on the model performance are investigated by comparing the steady-state and dynamic simulation results as well as using linear analysis. Our analyses show that, for the SOFC under consideration, the temperature profiles in the fuel bulk flow, PEN, and interconnector can be approximated as one temperature layer. Therefore, the number of temperature states in each discretization unit can be reduced from 4 as in the baseline model to 2—the temperatures of the air bulk flow and solid structure—to reduce the order of the model while preserving the key dynamic characteristics of the SOFC. The model assuming only one temperature layer exhibits significantly larger error in dynamic responses compared to others.

It is noticed that, with a 16-unit discretization scheme, the SOFC model with the minimized number of temperature layers still has 160 states. The simplified model proposed here contains the same mass balance dynamics as the baseline model, which introduces eight concentration states for each discretization unit. Further model reduction is possible by approximating the gas flow dynamics using quasi-static relations, which is investigated in Ref. [19]. Optimizing the discretization scheme in the SOFC modeling could also contribute to the further simplification of the SOFC model. While we believe that similar conclusions can be drawn for counter- and cross-flow planar SOFCs, more in-depth analysis is also warranted to understand how different flow pattern might affect the modeling assumption. Finally, to improve the performance of SOFC systems, feedback control solutions will be developed in the future, based on the low-order model.

Table 6 Operating parameters for the case with SR pre-reformer

	Full load	Part load
Current load, I (A)	320	160
Ave. current density, $\bar{i}$ (A/cm^2)	0.8	0.4
Fuel utilization ratio	90%	90%
Pre-reforming ratio in SR pre-reformer	20%	20%
Steam-to-carbon ratio in SR pre-reformer	2	2
Inlet temperature of reformate to SOFC (K)	1023	1023
Air excess ratio	9	7
Inlet temperature of air to SOFC (K)	1023	1023

Acknowledgment

This work is supported in part by the Office of Naval Research under Contract No. N00014-06-1-0209 and US Army through TCN05158(SSP).

Nomenclature

A = cross area of the current path (m^2)
C_s = molar concentration of species s (mol/m^3)
I = electrical current load (A)
J = number of discretization units in the finite volume method
T = temperature (K)
∇T_{PEN} = PEN temperature gradient (K/cm)
U, U_{cell} = operating voltage of unit and cell, respectively (V)
U_{OCV} = open circuit voltage (V)
c_p = heat capacity of solid layers (J/K kg)
$c_{v,s}$ = heat capacity of species s (J/K mol)
d = channel height (m)
$h_s(T)$ = specific enthalpy of species s at temperature of T (J/mol)
i, $\bar{i}$ = current density and average current density, respectively (A/m^2)
$k_{f,\mathrm{PEN}}$, $k_{a,\mathrm{PEN}}$, $k_{f,I}$, $k_{a,I}$ = heat transfer coefficients from bulk flows to solid layers (J/K m^2 s)
l = length of spatial discretization unit (m)
$n_{\mathrm{in},s}$, $n_{\mathrm{out},s}$ = inlet and outlet molar flux of species s in a volumetric unit, respectively (mol/s m^2)
q_{cond} = heat conduction flux in solid layers (J/s m^2)
q_{in}, q_{out} = inlet and outlet enthalpy flux of gas flows in a unit, respectively (J/s m^2)
r_k = rate of reaction k (mol/s m^2)
u_{out} = outlet flow velocity (m/s)
ϵ = emissivity of solid layers
η = potential loss (V)
$\nu_{s,k}$ = stoichiometric coefficient of species s in reaction k
ρ = density (kg/m^3)
σ = Stefan-Boltzmann constant (W/m^2 K^4)

τ = solid layer thickness (m)

Subscript

I = interconnector
ox = oxidation reaction
red = reduction reaction
a = air flow
f = fuel flow
s_a = species in the air flow
s_f = species in the fuel flow
sol = solid structure in SOFC

Superscript

j = the jth discretization unit

References

[1] Singhal, S. C., and Kendall, K., eds., 2004, *High Temperature Solid Oxide Fuel Cells: Fundamentals, Design and Applications*, Elsevier Science, New York.

[2] Achenbach, E., 1994, "Three-Dimensional and Time-Dependent Simulation of a Planar Solid Fuel Cell Stack," J. Power Sources, **49**, pp. 333–348.

[3] Braun, R. J., 2002, "Optimal Design and Operation of Solid Oxide Fuel Cell Systems for Small-Scale Stationary Applications," Doctoral thesis, University of Wisconsin-Madison, Madison, WI.

[4] Petruzzi, L., Cocchi, S., and Fineschi, F., 2003, "A Global Thermo-Electrochemical Model for SOFC Systems Design and Engineering," J. Power Sources, **118**, pp. 96–107.

[5] Aguiar, P., Adjiman, C. S., and Brandon, N. P., 2004, "Anode-Supported Intermediate Temperature Direct Internal Reforming Solid Oxide Fuel Cell. I: Model-Based Steady-State Performance," J. Power Sources, **138**, pp. 120–136.

[6] Gemmen, R. S., and Johnson, C. D., 2005, "Effect of Load Transients on SOFC Operation-Current Reversal on Loss of Load," J. Power Sources, **144**, pp. 152–164.

[7] Sedghisigarchi, K., and Feliachi, A., 2004, "Dynamic and Transient Analysis of Power Distribution Systems With Fuel Cells-Part I: Fuel Cell Dynamic Model," IEEE Trans. Energy Convers., **19**, pp. 423–428.

[8] Xi, H., and Sun, J., 2005, "Dynamic Model of Planar Solid Oxide Fuel Cells for Steady State and Transient Performance Analysis," *Proceedings of ASME International Mechanical Engineering Congress and Exposition*, Orlando, FL, Nov. 5–11.

[9] Sorrentino, M., Guezennec, Y. G., Pianese, C., and Rizzoni, G., 2005, "Development of a Control-Oriented Model for Simulation of SOFC-Based Energy Systems," *Proceedings of ASME International Mechanical Engineering Congress and Exposition*, Orlando, FL, Nov. 5–11.

[10] Achenbach, E., 1995, "Response of a Solid Oxide Fuel Cell to Load Change," J. Power Sources, **57**, pp. 105–109.

[11] Aguiar, P., Adjiman, C. S., and Brandon, N. P., 2005, "Anode-Supported Intermediate Temperature Direct Internal Reforming Solid Oxide Fuel Cell. II: Model-Based Dynamic Performance and Control," J. Power Sources, **147**, pp. 136–147.

[12] Xi, H., and Sun, J., 2006, "Analysis and Feedback Control of Planar SOFC Systems for Fast Load Following in APU Applications," *Proceedings of ASME International Mechanical Engineering Congress and Exposition*, Chicago, IL, Nov. 5–10.

[13] Campanari, S., and Iora, P., 2005, "Comparison of Finite Volume SOFC Models for the Simulation of a Planar Cell Geometry," Fuel Cells, **5**(1), pp. 34–51.

[14] Xi, H., and Sun, J., 2006, "Comparison of Dynamic Planar SOFC Models With Different Assumptions of Temperature Layers in Energy Balance," *Proceedings of ASME International Mechanical Engineering Congress and Exposition*, Chicago, IL, Nov. 5–10.

[15] Iora, P., Aguiar, P., Adjiman, C. S., and Brandon, N. P., 2005, "Comparison of Two IT DIR-SOFC Models: Impact of Variable Thermodynamic, Physical, and Flow Properties. Steady-State and Dynamic Analysis," Chem. Eng. Sci., **60**, pp. 2963–2975.

[16] Mueller, F., Brouwer, J., Jabbari, F., and Samuelsen, S., 2006, "Dynamic Simulation of an Integrated Solid Oxide Fuel Cell System Including Current-Based Fuel Flow Control," ASME J. Fuel Cell Sci. Technol., **3**, pp. 144–154.

[17] Ota, T., Koyama, M., Wen, C., Yamada, K., and Takahashi, H., 2003, "Object-Based Modeling of SOFC System: Dynamic Behavior of Micro-Tube SOFC," J. Power Sources , **118**, pp. 430–439.

[18] Larminie, J., and Dicks, A., 2003, *Fuel Cell Systems Explained*, 2nd ed., Wiley, New York.

[19] Xi, H., and Sun, J., 2007, "A Low Order Dynamic Model for Planar Solid Oxide Fuel Cells Using On-Line Iterative Computation," ASME J. Fuel Cell Sci. Technol., to be published.

[20] Selimovic, A., 2002, "Modeling of Solid Oxide Fuel Cells Applied to the Analysis of Integrated Systems With Gas Turbines," Doctoral thesis, Lund University, Sweden.

[21] Franklin, G. F., Powell, J. D., and Emami-Naeini, A., 2002, *Feedback Control of Dynamic Systems*, 4th ed., Prentice-Hall, Englewood Cliffs, NJ.